JTTEE5 10:643-655

Deposition and Properties of High-Velocity-Oxygen-Fuel and Plasma-Sprayed Mo-Mo_2C Composite Coatings

L. Prchlik, J. Gutleber, and S. Sampath

(Submitted 2 October 2000)

Molybdenum thermal-spray coatings, dispersion strengthened by molybdenum oxides and molybdenum carbides, play an important role in industrial tribological applications. Traditionally, they have been prepared by plasma and wire flame spraying. High porosity and lower cohesion strength limit their application in situations where both galling and abrasion wear is involved.

In this study, high-velocity-oxygen-fuel (HVOF) deposition of molybdenum and molybdenum carbide coatings was attempted. Deposition was achieved for all powders used. Composition, microstructure, mechanical, and wear properties of the HVOF synthesized coatings were evaluated and compared with plasma-sprayed counterparts.

The HVOF coatings possessed a very good abrasion resistance, whereas plasma deposits performed better in dry sliding tests. Measurements showed a close relationship between the coating surface hardness and its abrasion resistance. Results also suggested correlation between molybdenum carbide distribution in the molybdenum matrix and the sliding friction response of Mo-Mo_2C coatings.

Keywords abrasion, decarburization, friction, HVOF, Mo_2C, plasma spraying

1. Introduction

Molybdenum-based coatings are traditionally used in a variety of sliding friction and wear applications. Since the hardness of pure molybdenum is low, its superior wear characteristic can be exploited better in dispersion-strengthened alloys. Strengthening with molybdenum oxides, molybdenum carbides, or chromium carbides can provide coatings with excellent scuff and wear properties.[1,2] Thermal spray processing represents an efficient way to deposit molybdenum alloys onto automotive components.[1,3] Wire flame and plasma spray techniques have been traditionally employed. In spite of a general belief that the heat input from a high-velocity-oxygen-fuel (HVOF) torch is insufficient for molybdenum melting, successful deposition of molybdenum and molybdenum oxide coatings by this technique has been reported.[4] Dense, hard coatings were prepared, but friction and wear properties were not explored. Higher density and hardness of HVOF deposits may potentially offer enhanced wear properties.

The main objectives of this study were as follows: (1) to investigate the possibility of depositing dense molybdenum-carbide coatings using the HVOF process; (2) to evaluate fundamental mechanical and frictional properties of the deposits in comparison with plasma counterparts; and (3) to understand the deposition mechanism involved in HVOF spraying of Mo-Mo_2C and clarify its implications for wear and friction response.

L. Prchlik, J. Gutleber, and **S. Sampath,** Center for Thermal Spray Research, Department of Materials Science and Engineering, State University of New York, Stony Brook, NY, 11794-2275. Contact e-mail: lprchlik@ic.sunysb.edu.

2. Experimental Procedures

2.1 Materials Selection and Processes

Plasma-sprayed coatings were prepared from commercially available Osram Sylvania SX 274 and SX 391 composite powders (Osram Sylvania Corp., Towanda, PA). These powders are produced by simultaneous agglomeration and carburization of crushed molybdenum in a reduction atmosphere followed by spray drying.[2] The SX 391 consists of pure hexagonal Mo_2C, whereas SX 274 is formed by a mixture of Mo_2C and residual molybdenum. The powders used for HVOF deposition were of similar compositions, but they were classified by the manufacturer in order to achieve a smaller particle size. The particle sizes and compositions for all powders used for plasma and HVOF spraying are listed in Tables 1 and 2, respectively. The morphology of the powders is shown in Fig. 1. A smaller particle size was desirable for the HVOF process because of lower flame temperature compared to plasma.

The plasma-sprayed deposits were produced under standard spraying conditions that are reported in Table 1. For the HVOF deposition, the HV 2000 Praxair gun (TAFA Inc., Concord, NH) was selected since the temperature of particles in flight are reported as being higher than those for other known available torches.[5] The HVOF spraying was optimized with respect to maximum deposition efficiency of the SX 391 powder by varying fuel/oxygen ratio. The resulting spraying conditions, with fuel-rich stochiometry, used for the sample preparation are listed in Table 2.

2.2 Characterization

The particle size distribution was evaluated with a particle size analyzer, Microtrac model SRA 200 (Microtrac Inc., Largo, FL). The information about the stream of particles during the de-

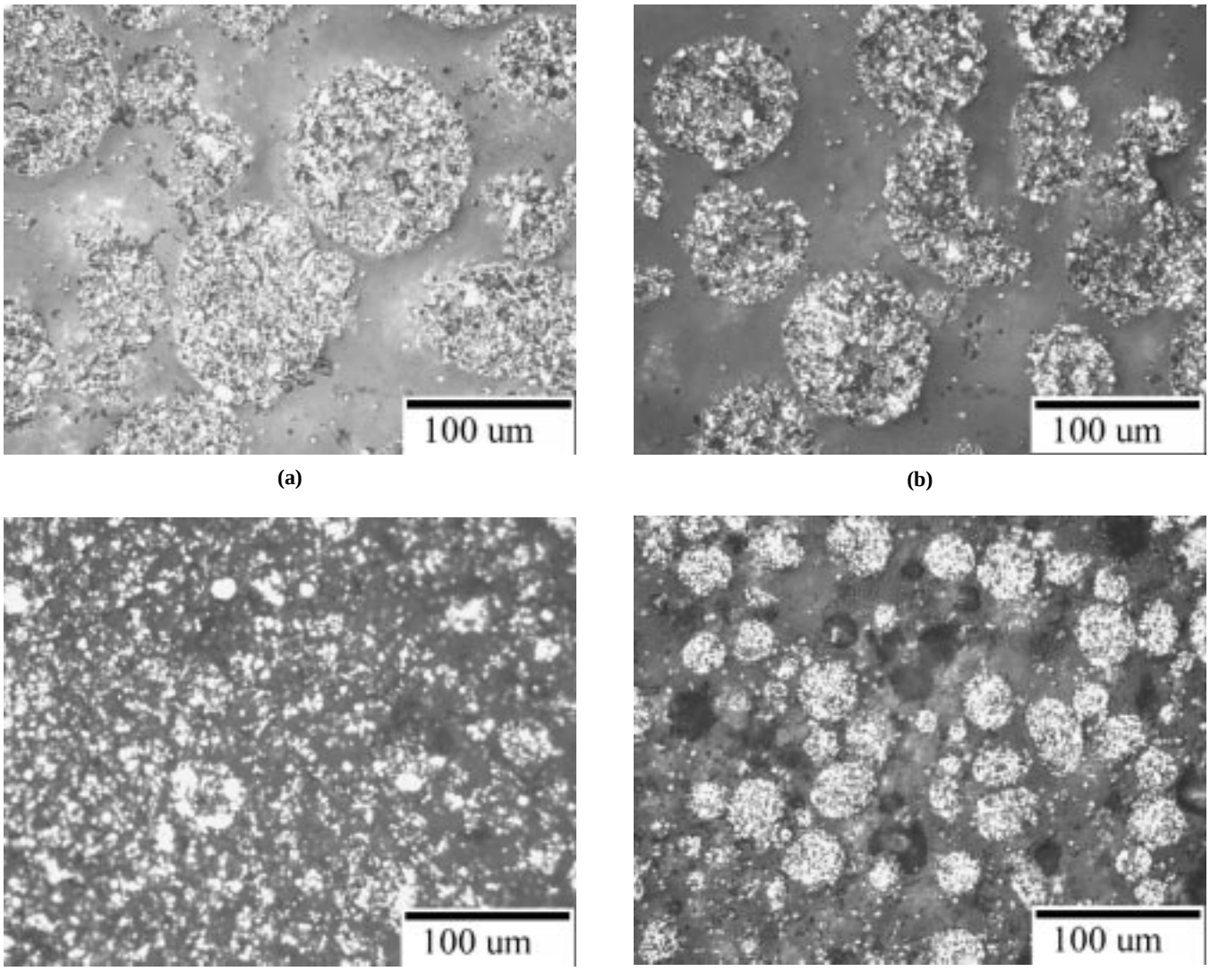

(a) **(b)** **(c)** **(d)**

Fig. 1 Optical micrographs of Mo-Mo_2C powders used in the study: (**a**) SX 274 plasma, (**b**) SX 391 plasma, (**c**) SX 274 HVOF, and (**d**) SX 391 HVOF

position was collected with a TECNAR DPV 2000 in-flight particle analyzer.

Coating samples prepared by standard metallographic techniques were used to evaluate numerous properties, such as microstructure, hardness, porosity, and the content of unmelted particles. Cross-section samples for optical microscopy were etched with modified Murakami's solution (1.4% $K_3Fe(CN)_6$ + 0.6% NaOH in H_2O). Wilson-Instron tester TU 230-C2550 (Instron, Wilson/Shore Instruments, Canton, MA) was used for hardness measurements. The duration of hardness tests was 15 s, and the reported values were averaged from a minimum of ten measurements. Hardness was measured on the cross sections (HV 25, 300 g) and on the surface of the samples prepared for wear testing (HV 1000 g). The microhardness measured at the lowest load (25 g) was used to estimate the actual hardness of the phases forming the splats.

X-ray diffraction was employed to reveal phase content, new phase formation, and the degree of decarburization of molybdenum carbide. All diffraction spectra were collected with a diffractometer, Philips type PW 1729 (copper radiation, step size 0.05°, Philips Electronic Instruments Corp., Mahwah, NJ). The correction of diffraction angle for accurate lattice-parameter measurements was achieved by standard alumina powder with known lattice constants. X-ray quantitative analysis was based on the direct comparison method using calculated intensity factors for Mo and Mo_2C.

2.3 Sliding Friction Testing

Room-temperature ball-on-disc friction and wear tests were performed on a modified Falex wear tester (Falex Corporation, Sugar Grove, IL) with the rotating sample positioned above the counterbody. In this configuration, a large portion of the debris produced was continually removed from the wear scar by the force of gravity. Since the interaction of the tested coatings with both metallic and ceramic materials was of interest, polished 440

Table 1 Materials and parameters used for plasma spraying of Mo-Mo_2C coatings

Plasma spraying			
Parameter		Description/Value	
Feedstock powders—composition	Particle size (μm)	(a) Osram SX 274—77% Mo_2C, 23% Mo	+49/−108
		(b) Osram SX 391—100% Mo_2C	+44/−96
Gun		F4-MB	
Gun nozzle		8 mm	
Gun power		500 A	
Gun voltage		69 V	
Primary argon gas flow		40 to 48 slpm	
Secondary hydrogen gas flow		8 to 10 slpm	
Carrier argon gas flow		2.5 slpm	
Total powder feed rate		40 g/min	
Vertical traverse speed		30 mm/s	
Spindle speed/diameter		160 rpm/140 mm	
Spraying distance		110 mm	
Deposition rate		approximately 2.5 μm/pass	

Table 2 Materials and spray parameters used for HVOF deposition of Mo-Mo_2C coatings

HVOF Spraying			
Parameter		Description/Value	
Feedstock powders—composition		Particle size (μm)	(a) Osram SX 274—55% Mo_2C, 45% Mo	+3/−48
			(b) Osram SX 391—100% Mo_2C	+13/−39
Gun			HV 2000	
Oxygen	Supply pressure		150 psi	
	Flow		600 scfh	
Propylene	Supply pressure		100 psi	
	Flow		160 scfh	
Nitrogen	Supply pressure		100 psi	
	Flow		45 scfh	
Powder feed rate			25 g/min	
Vertical traverse speed			6 mm/s	
Spindle speed/diameter			400 rpm/180 mm	
Spraying distance			230 mm	
Deposition rates			(a) 2 μm/pass	
			(b) 8 μm/pass`	

C steel and Si_3N_4 balls of 6.35 mm diameter were used as counterbodies. A constant normal force of 50 N was applied. The eccentric position of the ball and sample rotation (27.4 rpm) resulted in the sliding speed of 0.01 m/s over a wear scar of 7 mm in diameter. One-hour sliding tests represented approximately 36 m of effective sliding distance. A force transducer connected to a computer continually recorded the friction data. Prior to the friction testing, samples were polished with diamond discs and suspensions to final roughness, $R_a < 0.1$ μm; washed in methanol; and dried at 150 °C for 10 min. A minimum of two tests was performed for each material. Wear volumes were calculated from data obtained by a noncontact Zygo surface profilometer (Zygo Corporation, Middlefield, CT).

2.4 Abrasion Testing

Two-body abrasion tests were performed in the configuration depicted on Fig. 2. Three rectangular specimens (0.25 $in.^2$) were affixed to a rotating holder (40 rpm in same direction as disc with grinding paper), dividing the load evenly among the specimens. The 180 grit SiC paper, rotating at 300 rpm, was changed every 30 s. The load was adjusted so that the average pressure on each specimen was 80 kPa. Weight measurements were taken five times in 1 min intervals. The samples were washed quickly in ultrasonic bath to remove entrapped grit and dried for 10 min at 150 °C before the weigh measurements. Worn surfaces were examined using an ISI-SX-30 scanning electron microscope.

3. Results and Discussion

3.1 Coatings Deposition, In-Flight Diagnostics, and Microstructure

Significantly different deposition rates were measured for SX 274 and SX 391 Mo-Mo_2C powders (Table 2). The low deposition rate of SX 274 powder (2 μm/pass) compared to SX 391 (8 μm/pass) can be explained by fragmented powder geometry with large fraction of ultrafine particles (Fig. 1c). In fact, only a very thin coating (90 μm) was produced with the SX 274 powder for the same number of torch passes. Such a small thickness did not allow surface hardness and wear testing to be performed. The microstructure seemed to be less uniform than that of SX 391, and cracks parallel with substrate/coating interface were observed (Fig. 3).

From Fig. 4, it can be clearly seen that the SX 391 deposit consists of two regions with different microstructures. After etching, one type of region appears brighter in the photomicrographs than the other. Selective microhardness measurements showed that hardness of the bright region was as high

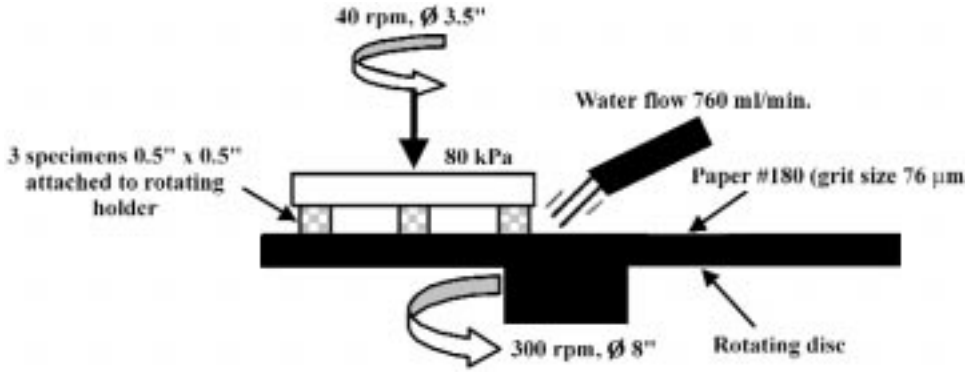

Fig. 2 Configuration of the wet abrasion test

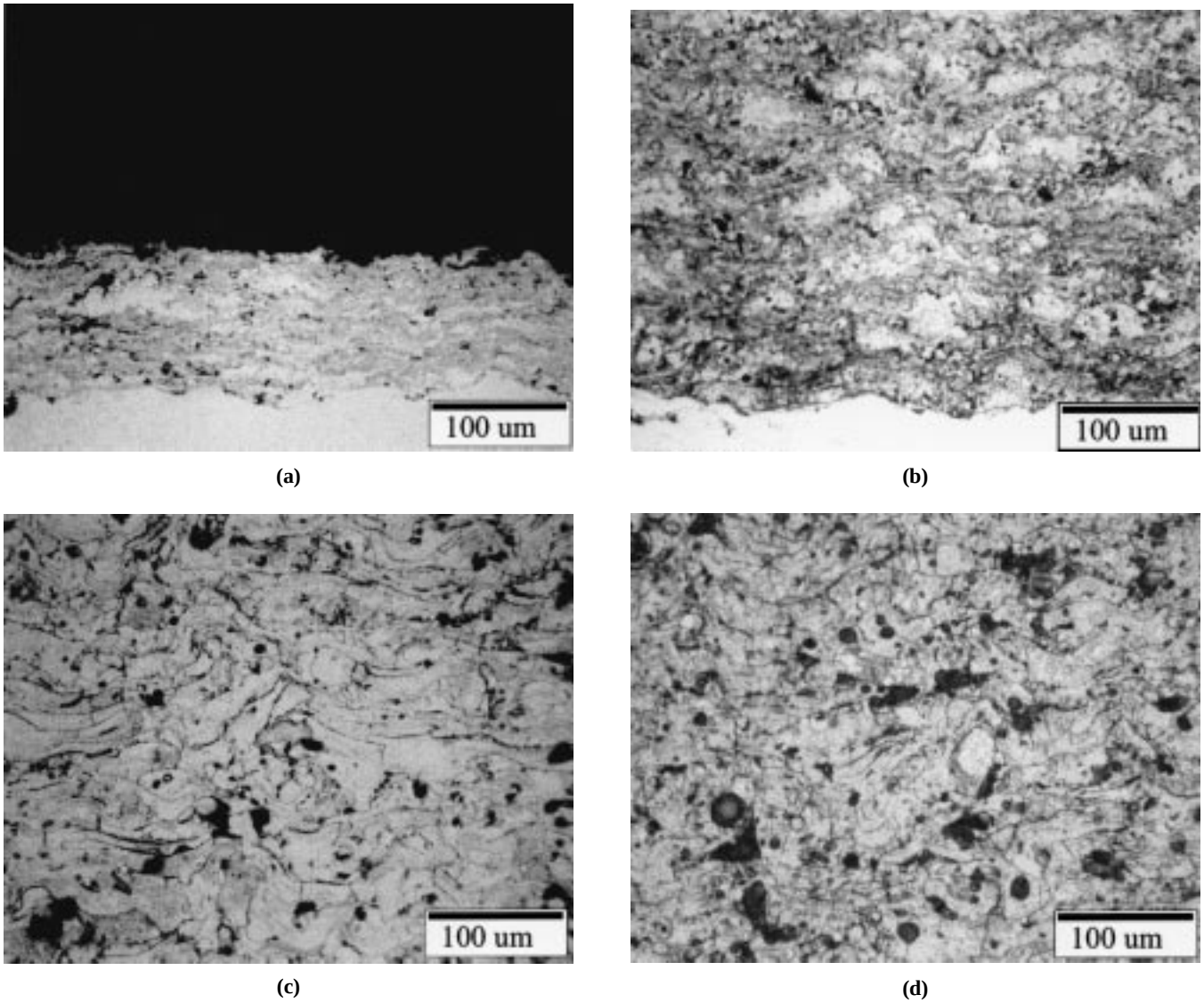

(a) **(b)** **(c)** **(d)**

Fig. 3 Optical micrographs of Mo-Mo_2C coatings: (**a**) SX 274 HVOF, (**b**) SX 391 HVOF, (**c**) SX 274 plasma, and (**d**) SX 391 plasma

as 1850 HV_{25}. This corresponds to the hardness of molybdenum carbide reported in the literature.[6] The second type of region has a typical splatlike morphology, appears darker on the photomicrograph, and has a microhardness of approximately 770 HV_{25}. The microstructure and hardness of this region suggests that the particles have undergone complete melting and decarburization during the deposition and formed molybdenum/molybdenum-oxide structure. The difference in hardness

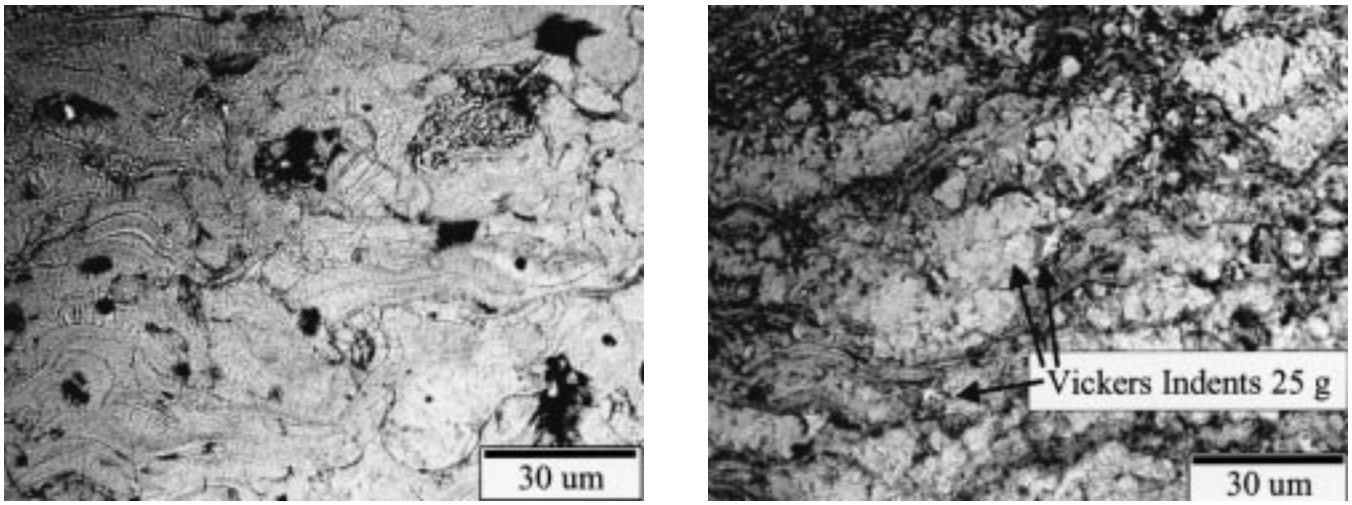

(a) **(b)**

Fig. 4 Comparison of microstructures of SX 391 deposited by different techniques: (**a**) plasma and (**b**) HVOF

Table 3 Results of diagnostics for HVOF spraying of Mo-Mo_2C powders

Technique powder	Microtrack (laser particle analyzer)	Tecnar (in-flight measurement)	
	Particle size (μm)	Velocity (m/s)	Temperature (°C)
Plasma SX 274 (Mo-Mo_2C)	76 ± 23	108 ± 24	3180 ± 176
Plasma SX 391 (Mo_2C)	64 ± 20	123 ± 26	3209 ± 158
HVOF SX 274 (Mo-Mo_2C)	23 ± 15	524 ± 65	2225 ± 135
HVOF SX 391 (Mo_2C)	38 ± 19	506 ± 75	2215 ± 105

Table 4 Overview of coatings prepared and their basic properties

Coating	Properties			
	Composition (wt.%)	HV_{1000} (g/mm^2) (surface)	HV_{300} (g/mm^2) (cross section)	HV_{25} (g/mm^2) (cross section)
Plasma SX 274	Mo, 19% Mo_2C	670 ± 36	660 ± 50	1320 ± 51
Plasma SX 391	Mo, 87% Mo_2C	590 ± 89	626 ± 157	1550 ± 112
HVOF SX 274	Mo	…	680 ± 105	…
HVOF SX 391	Mo, 55% Mo_2C	900 ± 21	890 ± 220	770 ± 152/1850 ± 105(a)

(a) Corresponds to light/dark regions observed in the optical micrographs (see text)

of these two regions can be seen from the size of the indents in Fig. 4.

The results of the in-flight diagnostic measurements for plasma and HVOF spraying are presented in Table 3. All measurements were conducted at the same standoff distances as those used for the coating deposition. The measurement illustrates a significant difference between the velocities of particles in the plasma and HVOF torches. Particles were traveling more than four times faster in the HVOF flame compared to the plasma. It can also be seen that particle velocities and temperatures were not strongly influenced by the type of powder sprayed but were dependent on the torch and spraying parameters used. Somewhat higher velocity of SX 274 particles in the plasma torch can be related to the smaller particle size of this powder.

Temperature of particles is one of the most important parameters controlling the deposit formation. From the coating microstructure and the particle temperature measure, it is clear that during plasma spraying the particles were fully melted when impinging on the substrate. For the HVOF, the temperatures recorded were significantly lower than those expected for melting of molybdenum (2650 °C) or molybdenum carbide (2400 °C).[6,7] In spite of this fact, deposition of both powders was achieved. Formation of Mo-Mo_2C eutectic is suggested as a mechanism for lowering the effective melting point to about 2200 °C.[8] A correlation between temperature and particle size of the SX 391 powder was investigated using the in-flight data. The analysis revealed that the average size of particles with temperature exceeding 2200 °C was only 35 μm, compared to 42 μm for particles having a temperature lower than the critical value. It suggests that mainly smaller particles were fully melted in the flame, whereas larger particles were melted only partially. The deposition of such particles was achieved by the high impact velocity and plastic deformation of softened material. This is confirmed by the small cross-section size of melted splats and larger regions having micromorphology similar to that of starting powders.

The overview of basic properties of all coatings investigated in this study is given in Table 4. The comparison shows that the

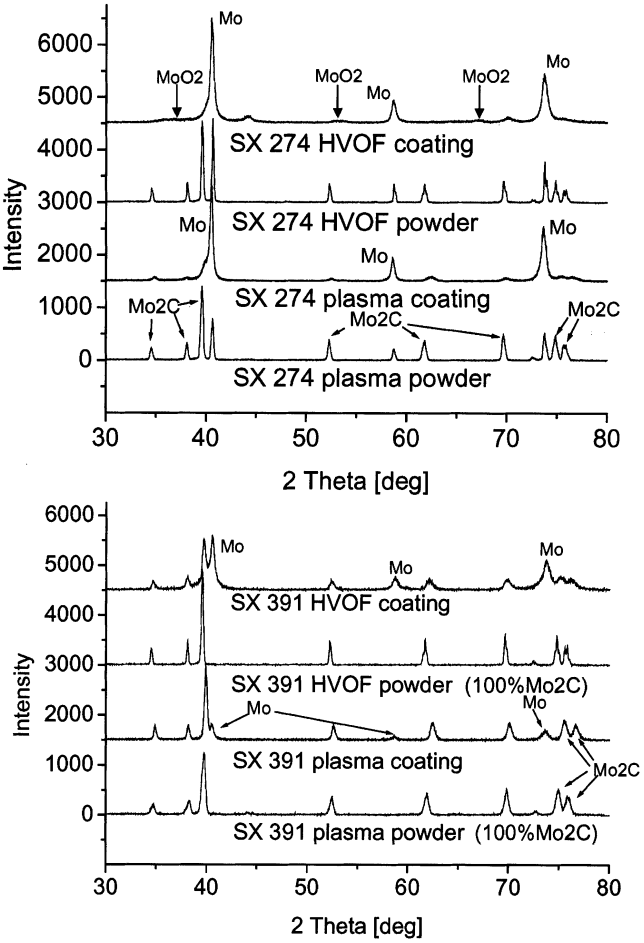

Fig. 5 X-ray diffraction spectra for HVOF and plasma-deposited Mo-Mo_2C systems

HVOF coating SX 391 had significantly higher hardness (HV_{300}, HV_{1000}) than its plasma-sprayed counterpart. Figures 3 and 4 show relatively uniform-lamellar microstructure of the plasma deposits with a very small amount of unmelted particles randomly distributed within the material. The difference in porosity between the HVOF and plasma SX 391 can be seen from the cross-section micrographs and is also visible in planar polished surfaces, as discussed later in Section 3.3. For plasma coatings SX 274 and SX 391, the microhardness values 1320 and 1550 HV_{25} were measured, respectively. Unlike in HVOF deposits, the hardness of the plasma deposits was reasonably uniform for different splats and regions of the coatings.

3.2 Decarburization and New Phase Formation

The diffraction data for SX 274 and SX 391 powders and coatings for both processes are shown in Fig. 5. Peaks present correspond to reflections from either bcc molybdenum or hexagonal molybdenum-carbide phases. The diffraction spectrum of the HVOF-coating SX 274 displays additional peaks corresponding to monoclinic molybdenum oxide, MoO_2. Furthermore, an intense diffraction peak at approximately 44.2° 2θ angle was observed that could not be attributed to either Mo_2C or any of the molybdenum oxide phases stable at the ambient temperature.[9] Only the cubic fcc Mo_3O phase reported in Ref 10 has an intense reflection close to this angle. Nevertheless, the existence of this low oxygen phase was not corroborated by more recent investigations.[9] The molybdenum/oxygen system is rather complex, and a large number of different oxide phases are reported. During HVOF spraying, the likelihood of formation of metastable phases is high; hence, the determination of exact oxide phases appeared to be beyond the scope of this study. The observed phenomenon is currently the object of an additional investigation.

A significant reduction of Mo_2C content was observed during spraying. The amount of molybdenum carbide in powders/coatings was quantitatively evaluated using a direct comparison method, and the results are summarized in Table 5. The reduction of carbide content was generally more pronounced in oxygen-fuel sprayed materials than in plasma-deposited ones. The degree of the decarburization/oxidation of particles in flame is generally dependent on the dwell time, surface/volume ratio, and partial pressure of the oxygen surrounding the particles. Taking the particle speeds and spraying distances into account, the dwell time appears to be twice as long for the plasma spraying compared to HVOF deposition. On the other hand, the surface/volume ratio is inversely proportional to particle size and is, therefore, two times larger for the particles used in the HVOF spraying. The observed difference in decarburization suggests that, in spite of the fuel-rich stochiometry, the atmosphere of the HVOF flame is more oxidizing than the environment of the plasma torch. Plasma spraying of SX 391 produced the least amount of decarburization (13%), whereas the HVOF SX 274 had the highest carbide loss (63%). The complete reduction of carbon from SX 274 during HVOF deposition is believed to be due to the fragmented geometry of the powder used and the correspondingly high surface/volume ratio.

The changes in lattice parameters for Mo_2C and Mo phases were evaluated. The results, summarized in Table 6, show that lattice constants of Mo_2C were smaller in deposits than in powders. The decrease was more significant in the *a* direction than in the *c* direction. Qualitatively, the same behavior was observed for both spraying techniques, even though this effect was more prominent in plasma-sprayed coatings. It should be mentioned that the comparison for plasma SX 274 has somewhat lower significance due to low carbide content, and correspondingly, small signal/noise ratio of diffraction peaks complicating a reliable position evaluation. The molybdenum-carbide hexagonal phase can exist within a relatively wide composition range with a carbon content lower than the one corresponding to the ideal stochiometry (approximately 6.25 wt.% of C).[6,7] A decrease in lattice parameters of molybdenum carbide is connected with the reduction of the carbon content.[11,12] Smaller lattice parameters of Mo_2C, therefore, were an indication of the reduction of carbon content in its lattice.

A close examination of shapes of diffraction peaks of Mo_2C present in HVOF SX 391 coating shows that the peaks display a large split that cannot be explained by contributions from $K_{\alpha 1}$ and $K_{\alpha 2}$ radiation (well visible for peaks with $2\theta > 69°$). The observed peaks are formed by contributions from carbides of two types with markedly different lattice parameters and corresponding variation of carbon content. The diffraction spectrum is then a superposition of the spectra from the two distinct microstructure regions, discussed in Section 3.1 as dark and light regions. Molybdenum carbide present in the first type of region

Table 5 Comparison of reduction of molybdenum carbide contents for different spraying techniques and starting powder compositions

Spraying technique	Material	Mo_2C content (wt.%)		Material	Mo_2C content (wt.%)	
		Powder	Coating		Powder	Coating
Plasma	SX 274	77	19	SX 391	100	87
HVOF	SX 274	63	0	SX 391	100	55

Table 6 Lattice parameter change for selected powders and corresponding deposits

Material/technique	Phase	Lattice constant	Powder (10^{-1} nm)	Coating (10^{-1} nm)	Change (10^{-1} nm)	Change in (%)
SX 274 plasma	Mo_2C	*a*	3.002	2.967	−0.035	−1.17
	Mo_2C	*c*	4.716	4.721	0.005	0.11
	Mo	…	3.145	3.150	0.005	0.16
SX 274 HVOF	Mo_2C	*a*	3.005	…	…	…
	Mo_2C	*c*	4.738	…	…	…
	Mo	…	3.147	3.147	0	0
SX 391 plasma	Mo_2C	*a*	3.010	2.975	−0.035	−1.17
	Mo_2C	*c*	4.737	4.721	−0.016	−0.35
	Mo	…	…	3.150	…	…
SX 391 HVOF	Mo_2C	*a*	3.007	2.985	−0.023	−0.75
	Mo_2C	*c*	4.730	4.729	−0.0005	−0.01
	Mo			3.146		

Table 7 Wear and friction data for various coatings and balls

Load: 50 N	Steel 440 C ball, ∅ 6.35 mm				Si_3N_4 ball, ∅ 6.35 mm			
Duration: 1 h	Wear (10^{-3} mm^3)		COF after		Wear (10^{-3} mm^3)		COF after	
Material	Scar	Ball	2 m	35 m	Scar	Ball	2 m	35 m
SX 274 plasma	5.5	0.2	0.18	0.19	6	1.6	0.2	0.5
SX 391 plasma	4.0	0.7	0.18	0.19	7.7(a)	1.9	0.21	0.35
SX 391 HVOF	4.8(a)	1.6	0.5	0.65	7.4(a)	9.8	0.68	0.55

(a) Estimate of wear volume complicated by irregular scar profile and pileup of debris

is surrounded by fully melted molybdenum, has a low carbon content, and has smaller lattice parameters. The second type of region is represented by carbides that have not been fully melted during the deposition and so have not undergone such a significant change in carbon content and lattice constants.

Conversely, the lattice constant of molybdenum present in the SX 274 plasma coating is significantly larger than that in the starting powder. It is well known that the interstitial carbon expands the molybdenum lattice.[13] Linear extrapolation of lattice-parameter/carbon-content dependence measured in Ref 13 (for observed 0.16% expansion of Mo lattice) yields a carbon content in Mo-C solid solution of 0.1%. The equilibrium solubility of carbon at room temperature is limited to less than 0.03%.[6,7,14] High carbon content (up to 0.5%) and large changes of molybdenum lattice parameters (up to 0.32%) were reported by the authors of Ref 2, where the expansion of Mo lattice was attributed to its supersaturation with carbon after rapid solidification. This demonstrates that during plasma spraying the diffusion in melted Mo-Mo_2C is sufficient to redistribute carbon within a flying particle. On the other hand, the lattice of molybdenum present in the HVOF deposits is not significantly larger than that in starting powders, which means that most carbon was removed from small particles in-flight.

Based on the microstructure observations and x-ray diffraction measurements, some basic differences between HVOF and plasma deposition of molybdenum carbides can be seen. In the plasma spraying, the majority of particles are fully melted, which enables effective diffusion of carbon between carbides and molybdenum. Upon impact, a supersaturated, molybdenum solid solution containing fine molybdenum carbide crystals is formed by rapid solidification. This was confirmed by the transmission electron microscopy (TEM) observation. The bright-field image in Fig. 6 shows globular molybdenum-carbide crystals with size of approximately 100 nm. The distribution of the fine crystals is very uniform, which explains why the microhardness within the splats varies only slightly.

In the flame of the HVOF torch, the small particles of SX 391 powder melt, lose a large portion of carbon, and form molybdenum regions with small carbon content and low hardness. Molybdenum carbide is present in smaller quantity within these regions, but a large portion of it is deposited directly by mechanical impact, as discussed in Section 3.1. The molybdenum carbides deposited by mechanical impact are not so carbon deficient since the diffusion in the core of the particles is very limited. These two distinct deposition mechanisms make the structure of HVOF deposit heterogeneous.

3.3 Wear Testing

The wear test results for both types of counterbodies are presented in Table 7. The comparison of friction data and wear volumes reveals a basic difference in friction behavior of plasma

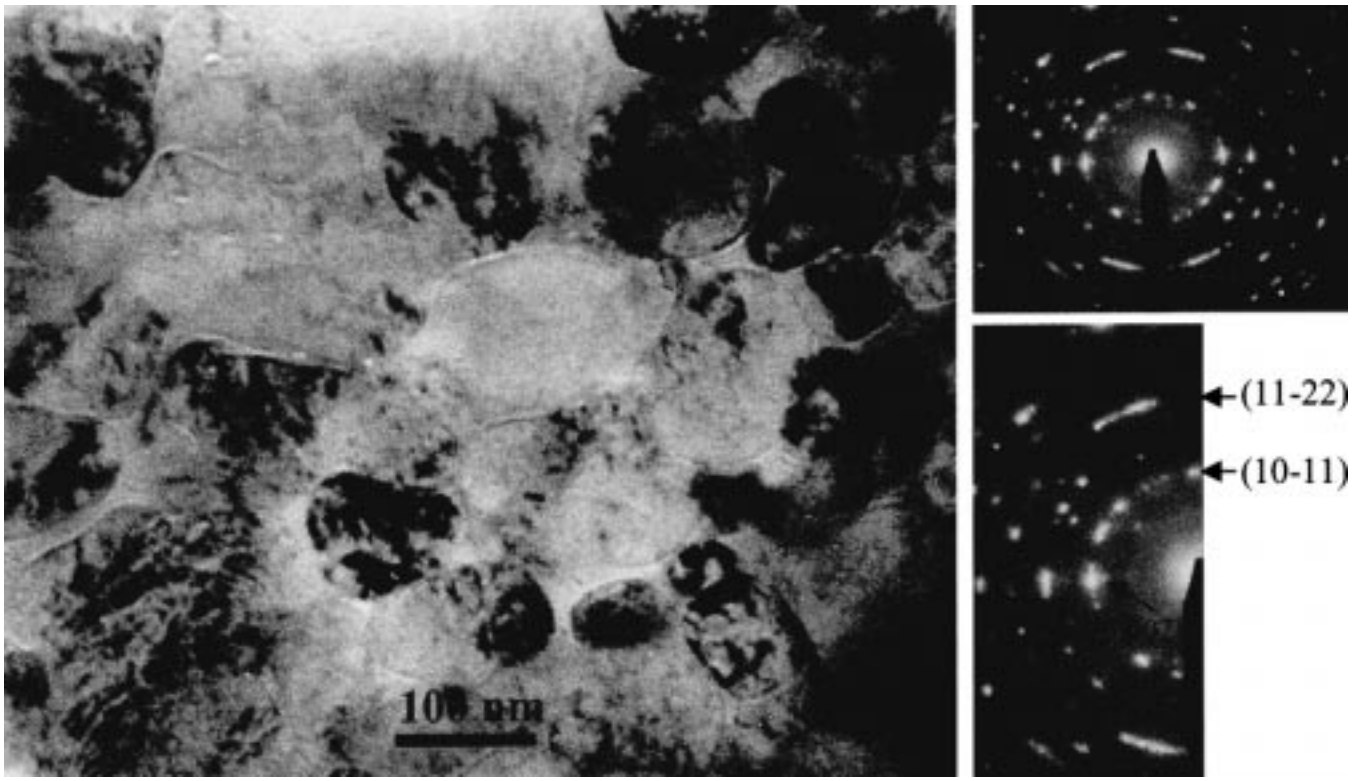

Fig. 6 Bright-field TEM image of plasma-sprayed SX 391 Mo-Mo_2C showing distribution of globular carbide particles in molybdenum matrix (87% of molybdenum carbide); diffraction pattern from Mo_2C-rich area

and HVOF coatings. For all plasma-sprayed coatings tested against the steel balls, the coefficient of friction (COF) remained lower than 0.2 during the entire test, as can be seen on Fig. 7. On the other hand, the COF for HVOF coatings tested against the same counterbody almost immediately reached the value of approximately 0.5. In the case of Si_3N_4 balls, a gradual increase of the COF with time was observed for all coatings. For SX 274 and SX 391 plasma coatings, the COF reached values of 0.5 and 0.35 at the end of the test, respectively. In spite of lower porosity of the HVOF coating, the increase of the COF (tested against Si_3N_4 ball) was much more rapid and reached its maximum value of 0.68 at the early phase of the test. Figure 8 shows the comparison of wear scars for HVOF and plasma SX 391 coatings tested against both types of counterbodies. The HVOF SX 391 coating exhibits more signs of intense adhesive wear compared to plasma materials. Also, the wear of balls was larger when in contact with HVOF-sprayed materials.

To explain the observed difference, an interrupted test, including observation of wear scars and balls in 40 s time intervals, was performed on the plasma and HVOF SX 391 coatings. Figure 9 shows that after the same distance the appearance of the wear scars of both materials was different. After 40 s (0.4 m), almost no surface damage could be observed in the case of the plasma coating, whereas the HVOF coating displayed some localized delamination. It should be noted that the original polished surface of the plasma coating prior to the test shows a large amount of surface voids (in-plane size 10 to 100 μm), whereas the original surface of HVOF coating has a smooth surface with limited number of voids (in-plane size <20 μm). In time intervals of 80, 120, and 160 s, the comparison of surface conditions was not significantly different from the first observation. A larger surface damage to the plasma coating was noticed after 320 s (3.2 m) of sliding. This damage had a form of cutting and plastic deformation. For the HVOF coatings, the damaged zones and the surface roughness increased, causing the rapid rise of the COF to 0.68. Etching of the surface of the HVOF coating with Murakami's etchant showed that the delaminated areas represented the edges of hard but brittle molybdenum-carbide zones. At the same time, an intense transfer film formation was observed on the surface of the HVOF test specimens. When illuminated in the optical microscope, a colored diffraction pattern was formed in the areas of transition films. The film appears as a gray area on the presented black and white micrographs. The formation of the film suggests that an intensive adhesive action was taking place during sliding and contributed to the high values of the COF for the HVOF coatings. It is speculated that the more intense adhesive wear of HVOF deposited molybdenum may be related to its low carbon content compared to the plasma-sprayed materials, where no such film formation was recorded at this stage of sliding tests. After 25 min (15 m) of sliding, the first excessive delamination was recorded in the plasma coating, and the COF started to increase. This test showed that the first contact between the ball and the surface of the plasma coating produced localized plastic deformation with very limited material removal. Splat delamination and wear scar widening is postponed to a later phase of the test. In the case of HVOF, delamination and surface roughness rise occurs early in the test and causes the high value of the COF, characterized by the rapid increase of the scar width at the very beginning of the test and the large wear of its counterbody.

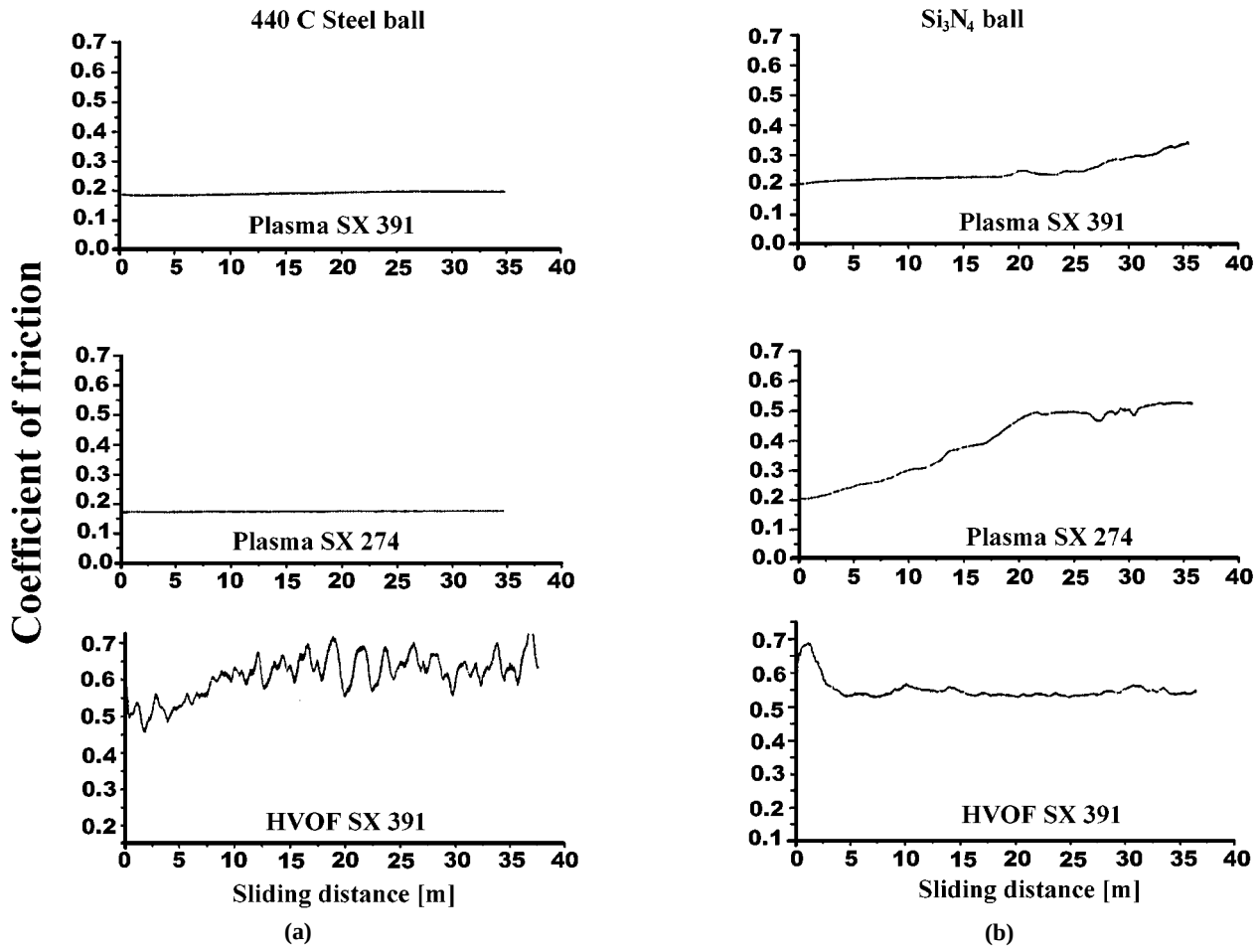

Fig. 7 The evolution of the COF for various coatings tested against (**a**) 440 C steel and (**b**) silicon nitride balls

These results suggest that the differences in coating microstucture, such as nonuniform distribution of Mo_2C in HVOF coating and strong molybdenum supersaturation by carbon of the plasma coatings, are responsible for different friction properties. It is believed that the main reason for significantly different friction behavior between the HVOF coatings and the plasma-sprayed ones is the difference in the strengthening mechanism of both structures. The splats in the plasma deposit are compact, formed by nanosized, globular molybdenum carbides with a reduced carbon content and lower hardness embedded in the molybdenum matrix, which is supersaturated by carbon. This compact structure can well resist even the contact loading in the initial stage of ball-on-flat sliding, when the Herzian stress is very high. On the other hand, the HVOF coatings contain a large amount of unmelted carbide particles with very high hardness. Carbides in these hard regions are not so uniformly bound by the molybdenum matrix. The structure of the HVOF Mo_2C regions is hard yet brittle and can be partially delaminated during the initial stage of the sliding contact.

3.4 Abrasion Testing

The chart in Fig. 10 reveals a striking difference between the abrasion resistance of the materials tested. The SX 391 plasma-deposited coating has a very low abrasion resistance, while the HVOF counterpart performance was significantly superior. For comparison, the weight losses of 440 C steel and sintered alumina in similar tests are 190 and 12 g/mm^2 min, respectively.

The difference can be explained by the observation of the SEM micrographs. The low abrasion resistance of SX 391 plasma coating was caused by the delamination of entire splats, while the weight loss of HVOF SX 391 was caused mainly by cutting action. Even though a localized delamination in the molybdenum carbide areas occurred also for HVOF coating, the remaining core parts of the molybdenum carbide regions were slowing the cutting action of SiC grains. The overall abrasion rate was in this way reduced. In plasma SX 274 coating, a mixed mechanism of material removal was observed, including cutting and delamination similar to plasma SX 391.

4. Conclusions

Molybdenum carbide powders were successfully deposited with a HVOF technique. The degree of decarburization during the combustion spraying was higher than in the case of plasma spraying.

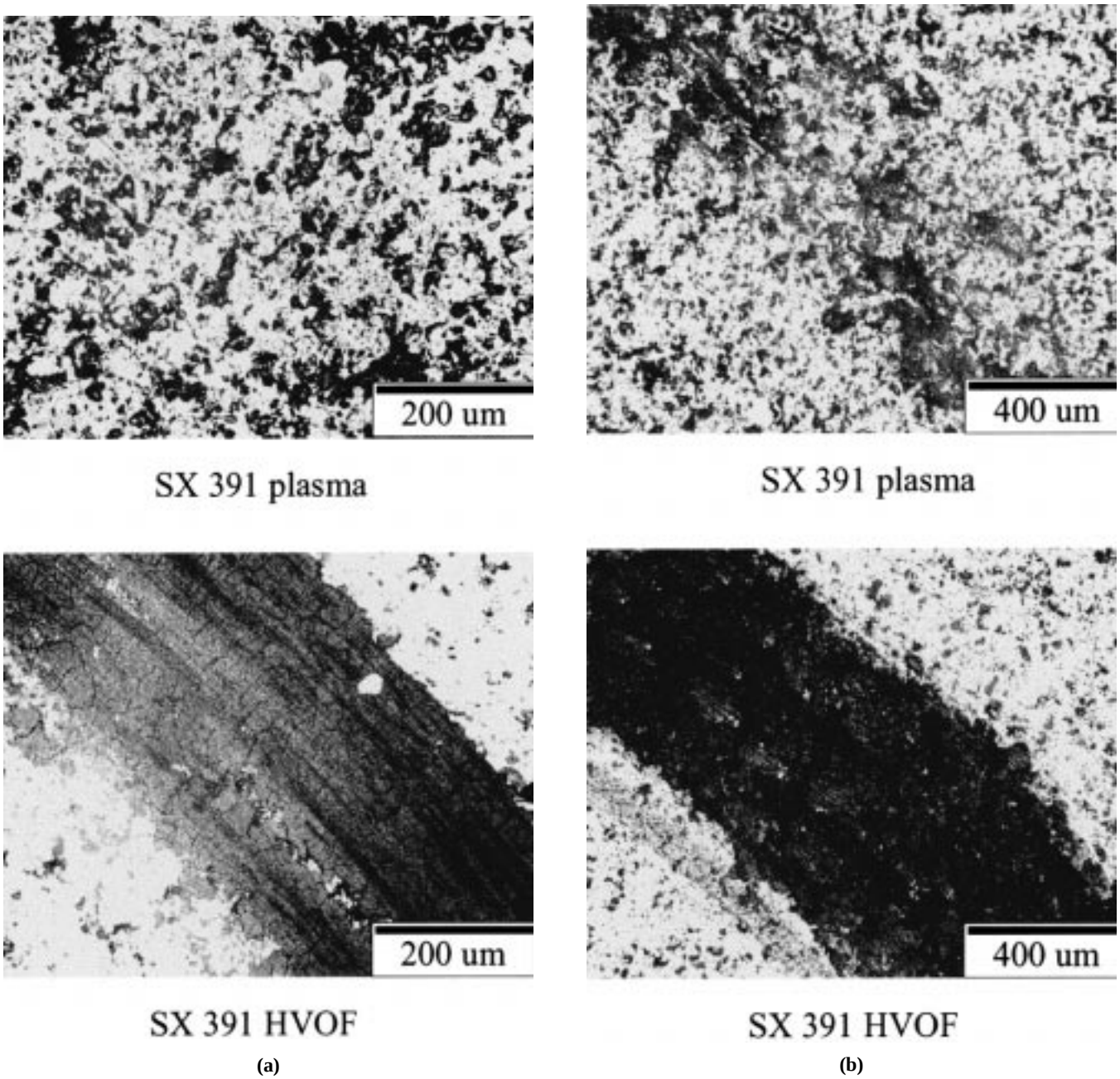

Fig. 8 Surface of wear scars for HVOF and plasma SX 391 Mo-Mo_2C tested against (**a**) 440 C steel and (**b**) silicon nitride balls

Lattice constants of molybdenum present in HVOF and plasma deposits were significantly different. Molybdenum formed in the plasma splats was strongly supersaturated by carbon. A similar effect was not observed in HVOF deposits. Molybdenum carbides had smaller lattice constants in the plasma deposits, which is believed to be due to dissolution of carbon in the Mo matrix during the deposition melting and subsequent entrapment of carbon in molybdenum lattice upon rapid solidification.

The HVOF coatings had higher density and hardness values; nevertheless, their sliding friction properties in the tests performed did not appear to be superior to the traditional plasma-sprayed materials. The main difference consisted in the very low COF of the plasma deposits and a rapid onset of the high COF for the HVOF coatings. This difference was attributed to the highly heterogeneous structure of the HVOF materials with the high content of hard yet brittle molybdenum-carbide regions.

At the same time, the abrasion resistance of HVOF SX 391 Mo-Mo_2C was more than ten times higher than that of a coating prepared from an equivalent powder by plasma spraying. In the plasma coatings, thinning and subsequent delamination of entire splats or their parts was the mechanism controlling the wear rates. Even though localized delamination from molybdenum carbide regions in HVOF SX 391 occurred as well, it produced

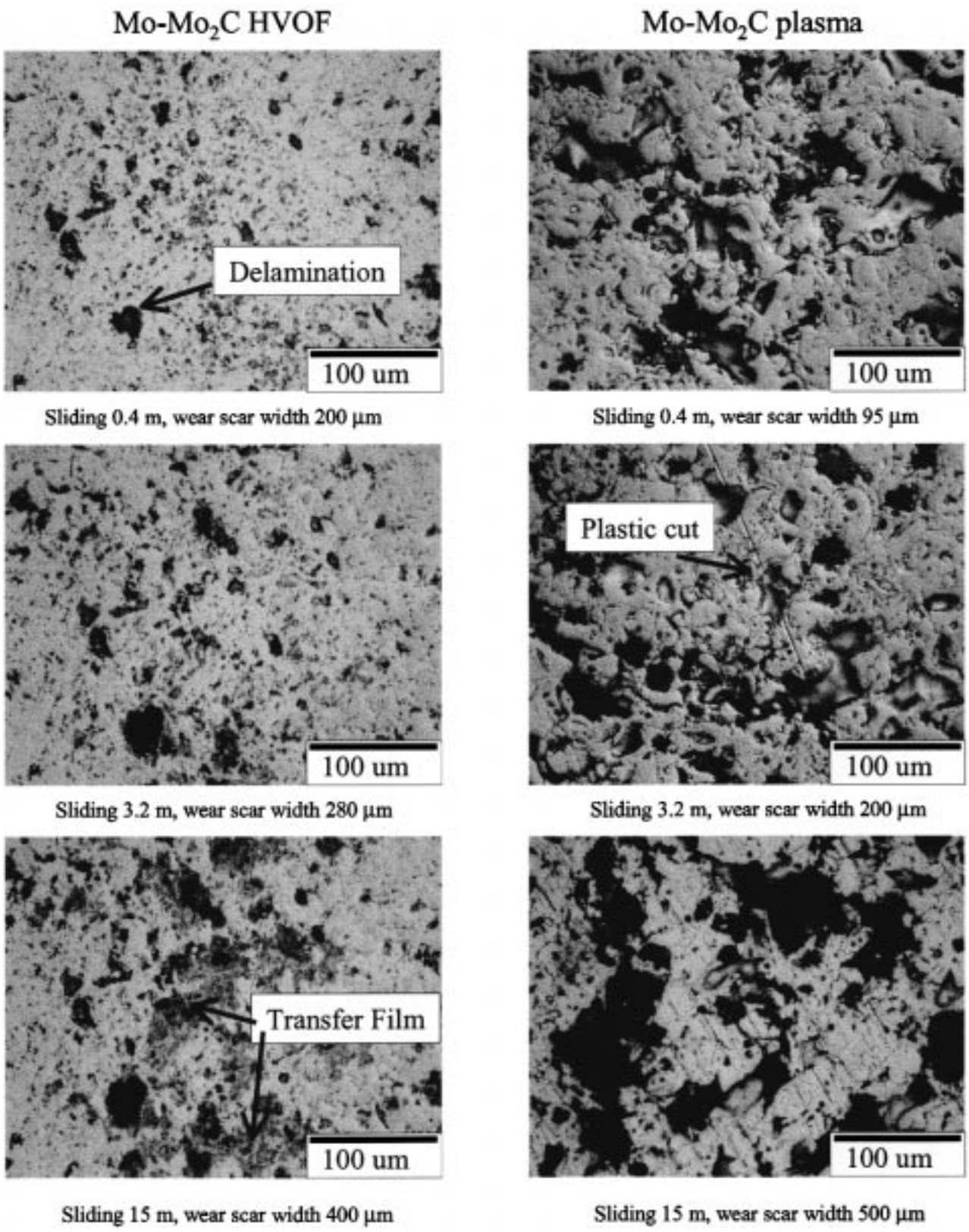

Fig. 9 Different stages of dry wear/friction tests of SX 391 plasma and HVOF-deposited coatings tested against silicon nitride balls

relatively small wear volumes compared to the debonding of entire plasma splats. The overall abrasion response of the HVOF-sprayed material was controlled by the hard Mo_2C phase rather than by the softer Mo matrix.

The study showed that the deposition of refractory carbide phase without a binder is possible by HVOF technique. Further development of Mo-Mo_2C HVOF spraying should be focused on improvement of the phase distribution in the coating structure,

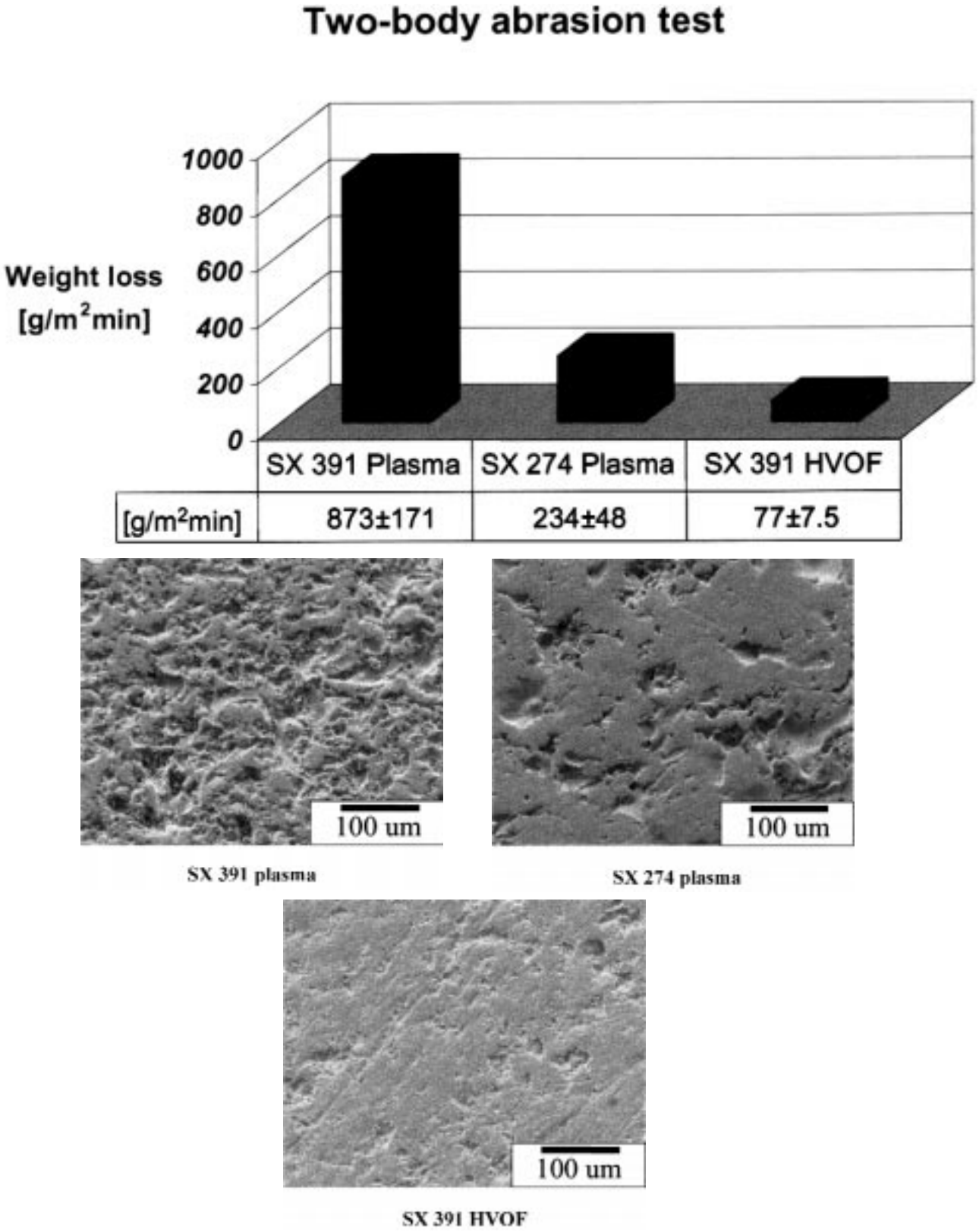

Fig. 10 Weight loss for different materials in two-body abrasion tests and corresponding SEM images of worn surfaces

which could then enhance its frictional characteristics and offer materials with excellent resistance to surface damage in different wear regimes.

Acknowledgment

This work was supported by the MRSC program of the National Science Foundation under Award No. 96-32570. The as-

sistance of OSRAM Sylvania with the powder separation for HVOF spraying is appreciated. Valuable comments of M. Blatchford and S. DePalo, as well as the TEM study performed by R. Goswami, are gratefully acknowledged.

References

1. F. Rastegar and A.E. Craft: *Surface Coatings Technol.*, 1993, vol. 61, pp. 36-42.
2. S. Sampath and S.F. Wayne: *J. Thermal Spray Technol.*, 1994, vol. 3 (3), pp. 282-88.
3. S.F. Wayne, S. Sampath, and S. Anand: *Tribol. Trans.*, 1994, vol. 37 (3), pp. 636-40.
4. H. Kreye and D. Blume: in *Thermal Spray: International Advances in Coatings Technology*, C.C. Berndt, ed., ASM International, Materials Park, OH, 1992, pp. 177-80.
5. J. Gutleber: Master's Thesis, State University of New York, Stony Brook, NY, 1999.
6. J.J. Liao, R.C. Wilcox, and R.H. Zee: *Scripta Metall. Mater.*, 1990, vol. 24, pp. 1647-52.
7. *Constitution of Binary Alloys*, M. Hansen, ed., McGraw-Hill, New York, NY, 1958, p. 370.
8. L. Brewer, R.H. Lamoreaux, R. Ferro, R. Marazza, and K. Girgis: in *Atomic Energy Review*, International Atomic Energy Agency, Vienna, 1980, pp. 285-89.
9. *Gmelin Handbuch der Anorganischen Chemie*, Main Series, 8th ed., Molybdaen, System No. 53, Ergaenzungsband Teil B1, Springer-Verlag, Berlin, 1975, p. 41.
10. N. Schoenberg: *Acta Chem. Scand.*, 1954, vol. 8, pp. 617-19.
11. A.A. Babad-Zakhryapin, M.I. Lagutkin, L.R. Borisov, and E.V. Borisov: *Met. Sci. Heat Treatment*, 1978, vol. 20, pp. 566-69.
12. W.P. Sykes, K.R. van Horn, and C.M. Tucker: *Trans. AIME*, 1935, vol. 117, pp. 173-86.
13. R. Speiser, W. Spretnak, W.E. Few, and R.M. Parke: *Trans. AIME*, 1952, vol. 194, pp. 275-77.
14. W.F. Few and G.K. Manning: *Trans. AIME*, 1952, vol. 194, pp. 271-74.